Permeation of Small Molecules through a Lipid Bilayer: A Computer Simulation Study

Daniele Bemporad and Jonathan W. Essex*

School of Chemistry, University of Southampton, Highfield, Southampton, SO17 1BJ United Kingdom

Claude Luttmann

Aventis Pharma S.A., 13 quai Jules Guesde F-94403 Vitry sur Seine Cedex, France

Received: May 8, 2003; In Final Form: January 19, 2004

To reach their biological target, drugs have to cross cell membranes, and understanding passive membrane permeation is therefore crucial for rational drug design. Molecular dynamics simulations offer a powerful way of studying permeation at the single molecule level, yielding detailed dynamic and thermodynamic data. Biological membranes have a very inhomogeneous character and a highly anisotropic behavior. Starting from a computer model proven to reproduce the physical properties of such a complex system, the permeation of small organic molecules across a lipid bilayer model has been studied. Free energy profiles and diffusion coefficients along the bilayer normal have been calculated for small organic molecules by means of all-atom molecular dynamics (MD) simulations constraining the compounds at chosen depths inside the membrane. These data also allow for the calculation of permeability coefficients, the results for which have been compared with experimental data. The calculated permeability coefficients are generally 1 order of magnitude larger than the equivalent experimental data, but the molecules' relative permeability coefficients are reproduced.

1. Introduction

For most of the routes of administration, cell membrane permeation is required for a drug molecule to reach the general circulation. Even after direct injection, or even if the drug can permeate via the paracellular route in the extracellular space, it soon encounters cell membranes to be crossed in order to reach its biological target. Most drugs cross cell membranes by passive permeation without the help of protein carriers, unless they are analogues of physiological substrates. An understanding of solute partitioning into biological membranes is then crucial for subcellular pharmacokinetics and rational drug design.[1]

Functional cell membranes are fluid mosaics of proteins within a lipid bilayer matrix.[2] Experimental and theoretical models for biological membranes, especially when studying solute permeation, are therefore phospholipid bilayers. Among them, much data have been collected for the dipalmitoylphosphatidylcholine (DPPC) bilayer.

The aim of this paper is to report the use of computer simulations to study small molecule permeation through a DPPC bilayer. Computer simulations can give atomic details which are not accessible from experiments and help to elucidate the mechanism of the passive permeation process at a molecular level.

2. Experimental Studies

Solute fluxes across lipid bilayers from a donor to a receiving chamber[3−10] or solute effluxes from or influxes into lipid vescicles[9,11−21] can be measured by means of radioactive tracers or fluorescence techniques. Apparent permeability coefficients P^{app} are then obtained by measuring the variation in time of the solute concentration in the acceptor compartment, since the concentration in the donor chamber is always much greater and assumed to be constant during the entire experiment. Since the barrier properties of the bilayer are shown to be pH independent, the observed pH dependence of P^{app} for electrolytes may be attributed to the different permeability coefficients of the neutral and ionic forms and to the relative fractions of permeant in neutral and ionized form with solution pH, as governed by the acid dissociation constant K_a. Assuming that only the neutral species crosses the membrane at a significant rate, the intrinsic permeability coefficient P_n^m of the neutral form of a weak acid or base through the membrane is[4−6,22−24]

$$\frac{1}{P^{app}} = \frac{C_{tot}}{P_n^m C_n} \tag{1}$$

where C_{tot} is the total solute concentration and C_n is the concentration of the neutral form depending on solution pH and solute K_a.

Permeation of molecules across membranes is thought to occur via the lipid bilayer by a three-step process involving the partitioning of the substance from the aqueous phase on one side into the bilayer, its diffusion across the bilayer, and its partitioning from the bilayer into the aqueous phase on the other side. This model is termed the solubility-diffusion model of permeation.[6−8,13,15,16,20,25−31] The overall membrane resistance R to solute permeation, defined as the inverse of the permeability coefficient P, can be expressed as the integral over the local resistances across the membrane:[20,23,27,29,32]

$$R = \frac{1}{P} = \int_0^d \frac{dz}{K(z)D(z)} \tag{2}$$

Here $K(z)$ and $D(z)$ are the depth-dependent partition coefficient from water into the membrane and the diffusion coefficient in the membrane at depth z, respectively, and d is the membrane

* To whom correspondence should be addressed. E-mail: J.W.Essex@soton.ac.uk.

10.1021/jp035260s CCC: $27.50 © 2004 American Chemical Society
Published on Web 03/20/2004

thickness. In what follows, the *z* axis is always taken along the membrane normal. Assuming, however, that transport is governed primarily by a distinct and uniform barrier region within the membrane, eq 3 simplifies to[20,23,29]

$$R = \frac{d_{\text{barrier}}}{K_{\text{barrier}} D_{\text{barrier}}} = \frac{1}{P^{\text{m}}} \tag{3}$$

where K_{barrier} and D_{barrier} are the solute partition coefficient from water into and the solute diffusion coefficient through the barrier region of the membrane, and d_{barrier} is the thickness of the barrier domain.

The value of K_{barrier} which contributes to P^{m} cannot be obtained from experiments of water/membrane partitioning, as a solute tends to partition into the region with the lowest solvation energy rather than into the barrier domain where the solvation energy is the highest. Fair correlations were obtained between the measured P^{m} and the solute partition coefficient K_{org} in reference organic solvents which are commonly chosen among 1-octanol or long-chain alkanes or alkenes, because of the hydrocarbon nature of the membrane interior. This is in accordance with Overton's rule stating that solute permeation through biological membranes is proportional to its partition in water/oil systems.[33] It is well-known that biomembranes differing in lipid composition, temperature, and level of hydration require different reference organic solvents,[3,14−16,19,25,26,28,34,35] primarily because these factors affect the lipid packing.

3. Calculation of Permeability Coefficients from Computer Simulations

The use of atomistic molecular dynamics (MD) simulations to calculate lipid membrane permeability coefficients was first applied by Marrink and Berendsen,[36,37] although the individual aspects of solute diffusion and partition through membrane mimetics (alkane slabs)[38−43] and lipid bilayers[44−47] have been also investigated separately by other authors. Marrink and Berendsen calculated permeability coefficients across a DPPC bilayer for water, oxygen, and ammonia. For each permeant, partition coefficients (rewritten in terms of free energy of transfer $\Delta G(z)$ from water into the membrane) and diffusion coefficients $D(z)$ were calculated by constraining the solute at chosen depths *z* inside the lipid bilayer. The overall resistance profile could therefore be obtained by applying directly eq 2.

The same method is applied here to calculate the permeability coefficients of eight small organic compounds representing some of the most common functional groups: acetamide, acetic acid, benzene, ethane, methanol, methyl acetate, methylamine, and water. This method requires the center of mass of the permeant particle to be constrained at chosen depths in the membrane and here it is referred to as the *z*-constraint method, since the normal to the lipid bilayer is taken along the *z* axis. By analogy with the SHAKE algorithm,[48] at each simulation step the equation of motion is solved without any constraint and then the atomic coordinates are corrected to satisfy the distance constraint between the center of mass of the solute and that of the lipid bilayer. The distance constraint is along the *z* axis only, corresponding to the bilayer normal, while the solute is completely free to move on the $x-y$ plane. The force required to maintain the constraint, acting along the *z* axis on the solute center of mass, is calculated at each MD step as

$$\boldsymbol{F}_i = m_i \frac{\Delta z}{(\Delta t)^2} \tag{4}$$

where m_i is the solute mass, Δz is the displacement covered by the solute along the *z* axis when solving the equation of motion (which is also the distance required to re-set its *z*-coordinates), and Δt is the simulation time step.

With one single computation, the *z* constraint allows for the calculation of both equilibrium and dynamic properties related to the permeation process.

The equilibrium property is the solute partitioning between water and different regions in the membrane and is expressed by the free energy of solute transfer from water into various depths *z* of the membrane, i.e., $\Delta G(z)$. The force acting on the center of mass of the solute at a chosen *z* depth is obtained at each time step as the negative of the force required to maintain the *z*-constraint and is indicated as $\boldsymbol{F}(z, t)$. Eventually, the free energy difference $\Delta G(z)$ between the water phase (outside the membrane) and depth *z* is accessible as the potential of the mean force

$$\Delta G(z) = -\int_{\text{outside}}^{z} \langle \boldsymbol{F}(z') \rangle_t \, \mathrm{d}z' \tag{5}$$

Here $\langle ... \rangle_t$ indicates an average over the simulation. When *z* is taken as the water phase on the other side of the lipid bilayer, the free energy profile for the entire membrane thickness is obtained. The solute $\Delta G(z)$ is related to its partition coefficient $K(z)$

$$K(z) = \exp(-\Delta G(z)/RT) \tag{6}$$

The dynamic property is the solute diffusion coefficient at different *z* depths in the membrane. Considering solute diffusion in a medium,[49,50] it can be demonstrated that the local time-dependent friction coefficient of the diffusant molecule $\xi(t)$ is related to the time autocorrelation function of the fluctuations of the instantaneous $\boldsymbol{F}(z, t)$ from the mean $\langle \boldsymbol{F}(z) \rangle_t$ with the following equation:

$$\xi(t) = \frac{\langle \Delta \boldsymbol{F}(z, t) \cdot \Delta \boldsymbol{F}(z, 0) \rangle}{RT} \tag{7}$$

Here *R* is the gas constant, *T* is the absolute temperature, and

$$\Delta \boldsymbol{F}(z, t) = \boldsymbol{F}(z, t) - \langle \boldsymbol{F}(z) \rangle_t \tag{8}$$

Assuming that $\xi(t)$ is large and decays rapidly compared to other time scales in the system, a satisfactory description of the full dynamics is provided by the static friction coefficient $\tilde{\xi}$:

$$\tilde{\xi} = \int_0^\infty \xi(t) \, \mathrm{d}t = \int_0^\infty \frac{\langle \Delta \boldsymbol{F}(z, t) \cdot \Delta \boldsymbol{F}(z, 0) \rangle}{RT} \, \mathrm{d}t \tag{9}$$

When studying diffusion across a free energy barrier,[49] the above condition is met if the slope of the free energy barrier over a distance covered by the particle during the decay time of its friction coefficient is lower than the thermal fluctuation, i.e., *RT* per mole. That is, the condition is met if the particle remains in a region of constant free energy. In this case, $\tilde{\xi}$ is related to the local diffusion coefficient $D(z)$ of the permeating solute at depth *z*

$$D(z) = \frac{RT}{\tilde{\xi}} = \frac{(RT)^2}{\int_0^\infty \langle \Delta \boldsymbol{F}(z, t) \cdot \Delta \boldsymbol{F}(z, 0) \rangle \, \mathrm{d}t} \tag{10}$$

Eventually, from $\Delta G(z)$ and $D(z)$ the overall resistance *R* to permeation is obtained according to the solubility-diffusion model by integrating over the local resistances $\mathscr{R}(z)$ at different

depths in the membrane

$$R = \int_{\text{outside}}^{z} \mathscr{R}(z')\,dz' = \int_{\text{outside}}^{z} \frac{\exp(\Delta G(z')/RT)}{D(z')}\,dz' = \frac{1}{P} \quad (11)$$

and the permeability coefficient P of the solute is defined as the inverse of R.

In this study, for each of the eight molecules simulated, 10 depths (z coordinates) were sampled from 0 to 30.5 Å from the bilayer center, constraining the solutes at those z depths. Results from one leaflet were considered valid for the other layer too, for reasons of symmetry.

4. Simulation Protocol

The simulation box contained 72 DPPC molecules arranged in a 2 × 36 bilayer, together with 2094 water molecules (full hydration). Lipids and water were modeled using version 27 of the CHARMM force field for lipids.[51] An equilibrated starting structure of the lipid bilayer was kindly obtained from A. D. MacKerell and S. E. Feller, who participated in developing the force field. The simulation protocol was the same as that used in some of the latest Feller simulations.[51,52] The Lennard-Jones (LJ) potential was switched smoothly to zero over the region from 10 and 12 Å. Electrostatic interactions were calculated via the Particle Mesh Ewald (PME) method using a κ value of 0.23 and a fast-Fourier grid density of ca. 1 Å^{-1}. The real space part of the PME summation was truncated at 12 Å. The SHAKE algorithm[48] was used to constrain all covalent bonds involving hydrogens. The leapfrog algorithm[53] was employed to solve the equation of motion with a time step of 2 fs. A neighbor list, used for calculating the LJ potential and the real space portion of the PME, was kept to 14 Å and updated every 50 fs. Coordinates were saved every ps for subsequent analysis. Three-dimensional periodic boundary conditions were applied. Only the cell length normal to the membrane (L_z) was allowed to vary during the simulation to maintain a constant normal pressure (P_N) of 1 atm. The other cell dimensions (L_x and L_y) were constrained to maintain a constant surface area per lipid (A) of 62.9 Å^2. The pressure was maintained by the Langevin Piston algorithm[54] with a mass of 500 amu and a collision frequency of 5 ps. The temperature (T) was maintained at 50 °C, well above the phase transition temperature of DPPC bilayers, by means of the Hoover thermostat.[55] A value of 1000 kcal ps^2 was used for the thermostat (fictitious) mass. The ensemble was therefore NP_NAT.

Topologies and parameters for the small organic solutes were available from the latest CHARMM force field for lipids and proteins. The molecules were manually inserted in the lipid bilayer at the desired z depth and a crude short minimization was performed to eliminate bad contacts. The steepest descent algorithm was employed for the minimizations.

For each z depth, 5 xy positions on the bilayer plane were sampled, this giving a total of 10 × 5 = 50 different positions sampled for each molecule. In a single simulation, only 5 of the 10 z depths were studied, this leading to 50/5 = 10 simulations for each molecule. In other words, each single simulation contained 5 solutes whose center of mass was constrained at 5 different depths distributed over both leaflets. Solutes were at least 6 Å apart from each other along the bilayer normal, but in most cases, they were more than 12 Å apart. Moreover, they were not in the same xy position but rather at five different positions on the bilayer plane. That is, only one solute was present at each z, and different xy positions for the same z were sampled in separate simulations. This care in choosing starting positions was expected to avoid strong solute−solute interactions and clustering. In each simulation, the 5 solutes were identical. Finally, 2.1 ns MD simulations were performed and the first 100 ps were discarded as equilibration. Therefore, for each molecule, P was calculated from 20 ns of simulations, and for the eight molecules, a total of 160 ns of data collection was performed.

All of the simulations were run in parallel with 4 processors, using version 27 of the CHARMM software package.[56] This software was modified to introduce the z-constraint algorithm described above. A few simulations were run on a cluster of PCs with 750 MHz AMD Athlon processors, but most were run on a cluster of PCs with 1000 MHz Intel Pentium IIIs and 1500 MHz Intel Pentium IVs.

5. Four Region Model

Since the membrane has a very inhomogeneous character when moving from one side to the other, each individual layer has been split into four regions as described in previous publications:[36,37]

Region 1: low headgroup density, 20−27 Å from the bilayer center.

Region 2: high headgroup density, 13−20 Å from the bilayer center.

Region 3: high tail density, 6−13 Å from the bilayer center.

Region 4: low tail density, 0−6 Å from the bilayer center.

The same distinction between membrane regions has been adopted here in the interpretation of the permeation results. In what follows, unless indicated otherwise, the x axis of all plots are along the bilayer normal, i.e., they report the z depths at which the molecules were constrained. The four regions into which each leaflet can be divided are also separated by vertical lines. Each lipid monolayer thickness is about 27 Å and further from the bilayer center there is bulk water. The sampled z depths in the simulations were the edges of the 4 regions and the middle position of each region. Since there are four regions, this yields eight z positions. Also the bilayer center itself (z = 0 Å) and a position in water phase (z = 30.5 Å) were sampled, giving a total of 10 z depths.

6. Free Energies

Free energy profiles $\Delta G(z)$ for the permeants studied, calculated with eq 5, are plotted in Figure 1. Errors in $\Delta G(z)$ are calculated by propagating the errors in the force $\boldsymbol{F}(z)$. The latter are standard errors calculated from the difference of the mean force $\langle \boldsymbol{F}(z) \rangle_t$ in each of the five individual simulations at each depth from their average.

6.1. Water. The free energy profile for water has the same shape as that in the original publication by Marrink and Berendsen:[36] $\Delta G(z)$ increases smoothly in region 1 and then very rapidly in regions 2 and 3, whereas region 4 present a small dip of 1.5 kJ mol^{-1} in the literature and 1.8 kJ mol^{-1} in these simulations. The increase in $\Delta G(z)$ is due to the loss of favorable electrostatic interactions and hydrogen bonds when leaving the bulk water phase for the hydrophobic core of the bilayer. In contrast, in the middle of the bilayer, $\Delta G(z)$ decreases because of the lower local density.

However, $\Delta G(z)$ values in these simulations are always about 3 kJ mol^{-1} lower than those reported by Marrink and Berendsen, with the exception of region 1. The highest value of $\Delta G(z)$ is reached in both simulations in region 4, but it is 26 ± 2 kJ mol^{-1} in the literature[36] and 22.9 ± 1.9 kJ mol^{-1} in these simulations. Since the bilayer core has the nature of long chain alkanes, Marrink and Berendsen compared this value with the

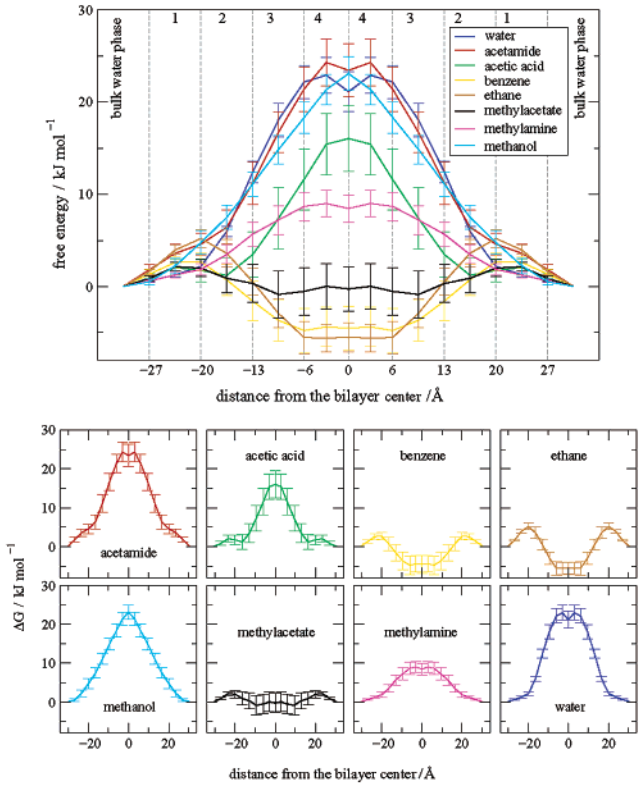

Figure 1. Free energy profiles. Top: bilayer is divided into the four regions. Bottom: for clarity, each profile is plotted alone. Error bars are standard errors calculated from the difference of the force in the five individual simulations from their average.

experimental $\Delta G°$ (water → hexadecane) result, which is 24.9 kJ mol^{-1}.[57] Values from these simulations are in fair agreement, although a little lower.

6.2. General Trend. Regarding the other solutes studied here, a general trend can be highlighted from Figure 1. For all of the compounds, $\Delta G(z)$ increases moving from the water phase into the membrane, crossing the headgroup regions 1 and 2. This is thought to be due to the increase in density, which makes the solubilization of a solute more difficult because of the lower free volume available to locate permeant molecules. The free energy then continues to increase in regions 3 and 4 for hydrophilic compounds, whereas it decreases for hydrophobic compounds. For the former, the hydrophobic core of the lipid tails represents the main barrier to permeation. For the latter, partition is more favored in the middle of the bilayer than at the lipid/water interface. Among the hydrophilic compounds, acetamide and methylamine show a small dip in $\Delta G(z)$ in the bilayer center as well as water, whereas acetic acid and methanol do not. Even though methyl acetate is a hydrophilic and polar compound (its ΔG(water → hexadecane) is positive), for the purpose of this analysis it is included among the hydrophobic compounds, since its $\Delta G(z)$ in the middle of the bilayer is lower than at the water/lipid interface. The explanation for this effect may reside in the fact that, in contrast to the other hydrophilic solutes, methyl acetate does not possess any hydrogen bond donors, or in other words it has no polar hydrogen atoms. The lipid headgroups do not possess any either. Therefore, methyl acetate is unique among the hydrophilic solutes in the sense that it can form no H-bonds with the surrounding lipids. The relationship between solute polarizability and size on one hand, and free energy of solute transfer from water into membrane models on the other, has been studied and reviewed extensively by Pohorille et al.[39,41,58−60]

In the following sections, the behavior of comparably sized solutes will be discussed.

6.3. Acetamide and Acetic Acid. The difference between the curves for acetamide and acetic acid resides primarily in region 1, where the acetic acid partition seems more favored than that of acetamide. A possible explanation may be due to the fact that the carboxylic group can form more favorable interactions with the highly charged phospholipid headgroups than can the amide group. Deeper in the membrane, the two curves have the same gradient and both reach their maximum value in region 4: 24.3 ± 2.5 kJ mol^{-1} for acetamide and 16.0 ± 3.6 kJ mol^{-1} for acetic acid.

The highest values of $\Delta G(z)$ calculated from these simulations for these two solutes are in fair agreement with their free energies of transfer from water into hexadecane and hexadecene: 18.6 and 17.7 kJ mol^{-1} for acetic acid respectively and 26.6 and 25.2 kJ mol^{-1} for acetamide respectively.[4,5,7,8,22,23]

Experimental acetic acid partition coefficients in water/lipid bilayer systems K(membrane → water) exist. It must be remembered that the zone of maximum partition accounts for only a very small fraction of the resistance to permeation and therefore K(membrane → water) is not the partition coefficient in the barrier region of the membrane. Acetic acid partition coefficients between cholesterol-free DMPC vesicles and water are reported to be around 1.5 for a wide range of temperatures in the liquid-crystalline phase.[14] This yields in turn ΔG(water → membrane) ≈ -0.45 kJ mol^{-1}. This is thought to correspond to the acetic acid partition into the headgroup region. In these simulations, acetic acid $\Delta G(z)$ is never negative, although considering the error bars $\Delta G(z)$ reaches the value of -0.7 kJ mol^{-1} in region 2. The protonation state of acetic acid as a function of depth inside the membrane is not accessible from experiments and, although in the membrane core, owing to its hydrophobic nature, the protonated state prevails over the ionized form, the behavior at the interface is unknown. The experimental K(membrane → water) mentioned above is strongly affected by such behavior, as the interface is thought to be the main site for the partitioning of acid compounds. However, as shown later, the main resistance to permeation comes from the membrane core, and as such, an accurate $\Delta G(z)$ at the membrane/water interface, although desirable, is not essential as its contribution to P is negligible.

6.4. Ethane. As expected for alkanes,[61,62] the ethane partition is favored in the hydrophobic core of the bilayer. The headgroup region of the bilayer, however, is highly charged, dense, and rich in water−lipid H-bond networks. Ethane partitioning in this region is then lower than in water. In the literature, ethane $\Delta G°$(water → hexadecane) is -4.6 kJ mol^{-1},[57] whereas $\Delta G(z)$ in region 4 from these simulations is -5.6 ± 1.5 kJ. Pohorille et al.[41] calculated $\Delta G(z)$ for methane along the normal of a bilayer made up of glycerol 1-monooleate molecules, which, with respect to a phospholipid, miss a second hydrocarbon chain and, above all, the highly charged phosphocholine group. Their profile was therefore negative at all depths and did not show the positive value across regions 1 and 2 as in these simulations. The lowest value of $\Delta G(z)$ in that publication was about -6.3 kJ mol^{-1}. Considering the differences in solute and membrane model, the agreement is satisfactory.

6.5. Methylamine and Methanol. Profiles for methanol and methylamine are very similar in regions 1 and 2. They are lower than ethane $\Delta G(z)$ in region 1 and at the beginning of region 2, because of the hydrophilic nature of these solutes. Methanol $\Delta G(z)$ is always higher than methylamine $\Delta G(z)$, but this difference is only significant in regions 3 and 4. Experimental

$\Delta G°$ (water → hexadecane) is reported to be 15.9 kJ mol^{-1} for methanol and 14.0 kJ mol^{-1} for methylamine.[57] From these simulations, the maximum value of ΔG(water → membrane) is 23.1 ± 1.8 kJ mol^{-1} for methanol and 9.0 ± 1.4 kJ mol^{-1} for methylamine, both reached in region 4. These results are not in quantitative agreement with experiment but do however correctly rank the compounds.

The experimental free energy of methanol transfer from water into DMPC liposomes in the liquid-crystalline phase is reported to be 3.18 kJ mol^{-1}.[63] This value is in agreement with those obtained in these simulations for region 1.

6.6. Methyl Acetate and Benzene. The $\Delta G(z)$ profile for methyl acetate is quite flat. Experimental methyl acetate $\Delta G°$(water → hexadecane) is reported to be 2.7 kJ mol^{-1}.[57] Calculated $\Delta G(z)$ in the middle of the bilayer for this compound ranges between 0.3 ± 2.0 and −0.9 ± 2.6 kJ mol^{-1} in regions 3 and 4. From the literature, ethyl acetate, which has an additional $-CH_2-$ group with respect to methyl acetate, has an experimental ΔG(water → membrane)[63] lower than its experimental $\Delta G°$(water → hexadecane),[57] suggesting that the simulation trend is correct.

Benzene $\Delta G(z)$ has a similar profile to that of ethane: $\Delta G(z)$ increases on entering the highly charged headgroup region and decreases moving deeper along the hydrocarbon tails. The experimental $\Delta G°$(water → hexadecane) for benzene is −12.3 kJ mol^{-1}.[57] The lowest $\Delta G(z)$ value from these simulations is −4.8 ± 2.4 kJ mol^{-1} in region 4. The calculated ΔG(water → membrane) is therefore higher than the experimental $\Delta G°$(water → hexadecane). This may be due to the fact that, because of lateral packing in lipid bilayers due to interfacial constraints which are not present in bulk organic solvents, accommodating a relatively larger solute such as benzene requires more work than accommodating the other smaller compounds studied in these simulations. Therefore, ΔG(water → membrane) for benzene deviates more from $\Delta G°$(water → hexadecane) than for the other compounds. This proves again that biomembranes do not behave like bulk solvents. Unfortunately, experimental values of benzene partition coefficients between water and lipid bilayers are not reliable for comparisons with these simulations, because of the benzene propensity to adsorb at the lipid/water interface.[34]

Although no rigorous free energy calculation was done, Stouch et al.[44] found that in un-constrained simulations at 320 K benzene shows no regional preference in the hydrocarbon part of a lipid bilayer (corresponding to regions 3 and 4 in this work), whereas at lower temperatures benzene concentrates in the bilayer center. Such findings are in agreement with the flat $\Delta G(z)$ profile found in these simulations in region 4 and part of region 3.

6.7. Data Convergence. The accuracy of the simulations was monitored by looking at the convergence of the value of $\langle F(z)\rangle_t$. $\langle F(z)\rangle_t$ s are plotted for water as an example in Figure 2 at z = 30.5 Å, when the solutes are still in bulk water, and z = 13.0 Å, which is in the densest part of the membrane and corresponds to the edge between the headgroup region and the hydrocarbon core of the bilayer. For the other depths, convergence profiles between these two extremes are found.

It can be seen that even a 2 ns simulation is not sufficient to ensure convergence, and this causes the significant errors in the $\Delta G(z)$ profiles. The permeant behavior is highly affected by those slow lipid motions which possess a long time scale and are not sampled completely in a single 2 ns MD simulation. This observation enforced the necessity of sampling the same z depth in several separate simulations at different $x-y$ positions, to obtain a reasonable value of $\Delta G(z)$ which is not too biased by the choice of the starting structure.

A favorable aspect is represented by the fact that at each depth the curves from the five simulations cross during 2 ns. This indicates that the independent simulations sample common regions of phase space and suggests that phase space, over the five simulations, is reasonably sampled.

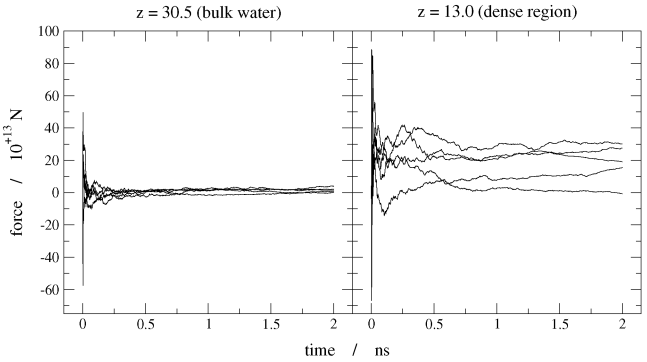

Figure 2. Value of $\langle \boldsymbol{F}(z)\rangle_t$ as a function of the simulation time from the five separate simulations.

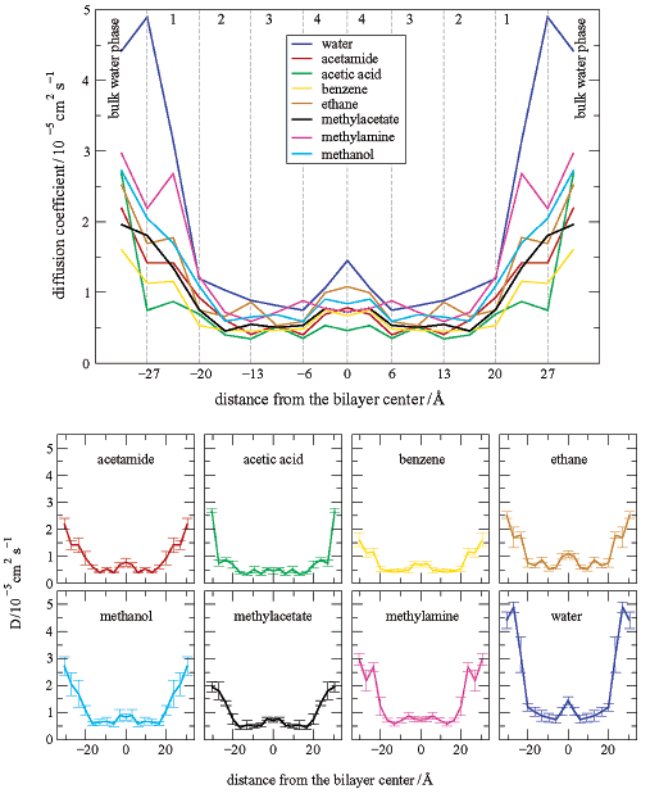

Figure 3. Diffusion coefficient profiles. Top: bilayer is divided into the four regions; for clarity error bars are not shown. Bottom: each profile is plotted alone with error bars. Error bars are standard errors calculated from the difference of the diffusion coefficients in the five individual simulations from their average.

7. Diffusion Coefficients

Diffusion coefficient $D(z)$ profiles for the permeants studied, calculated with eq 10, are plotted in Figure 3. Errors in $D(z)$ are standard errors calculated from the difference of the diffusion coefficients in each of the five individual simulation at each depth from their average.

7.1. General Trend. For all of the compounds, $D(z)$ decreases entering the membrane in regions 1 and 2, then it is quite uniform in region 3, and increases slightly in region 4. Diffusion coefficients inside the membrane are lower than in the bulk water phase because of the higher density of the lipid environment. Water, the smallest solute, has the highest $D(z)$ at all depths. However, the differences between the other permeants are very small and arguably not significant, as $D(z)$ of benzene, the largest solute, is not always the lowest.

7.2. Water. Marrink and Berendsen,[36,37] who introduced the *z*-constraint method, reported a water diffusion coefficient in the middle of the bilayer twice as large as in the bulk water phase, since in their simulations $D(z)$ increased very rapidly in regions 3 and 4. They reported the same behavior for ammonia and oxygen, and, since ammonia has a smaller size than water and oxygen has a larger one, the increase of $D(z)$ in regions 3 and 4 was even higher for NH_3 and lower for O_2. Values of $D(z)$ in the hydrophobic core of the membrane were found to be close to those in bulk alkanes such as hexadecane and cyclohexane. This result clearly indicated that size was the dominant parameter regulating diffusion in phospholipid membranes. In contrast, in these simulations, $D(z)$ is very similar for all of the compounds, whose sizes range from that of water to that of benzene, and $D(z)$ is lower than that in the bulk water phase at all depths. These differences may arise simply from the different potentials used and the fact that Marrink and Berendsen's simulations were run at 350 K.

7.3. Benzene. Our diffusion results are in closer agreement with other publications. Stouch et al.[44,45] simulated benzene diffusion at different depths in the hydrocarbon region of a DMPC bilayer and calculated its diffusion coefficient from the mean squared displacement. They reported $D(z)$ values of 0.46×10^{-5} cm^2 s^{-1} at the terminal methyl group of the lipid tails and 0.13×10^{-5} cm^2 s^{-1} at the carbonyl group between the fatty acid chains and the glycerol fragment, in both cases at 320 K. The simulations presented here yield values of 0.75×10^{-5} cm^2 s^{-1} in region 4 and 0.45×10^{-5} cm^2 s^{-1} in region 2. No experimental data are available about benzene $D(z)$ in lipid bilayers. Stouch et al. compared their values with those of di-*tert*-butyl nitroxide in dipalmitoyl lecithins,[19] which range between 0.05×10^{-5} cm^2 s^{-1} at the carbonyl position and 0.19×10^{-5} cm^2 s^{-1} at the chain terminal methyl. Therefore, Stouch's and these simulations yield values which are at most 1 order of magnitude higher than experiment, but both agree with experiment in reproducing faster solute diffusion in the lower than in the upper part of the lipid tails. The different value of $D(z)$ between these and Stouch's simulations may arise from the different way of calculating $D(z)$, and from the differences in the force field applied. Another important difference between this and Stouch's lipid systems is the free volume distribution: in Stouch's bilayer center voids large enough to host a benzene molecule were found.[44] It must be said that Stouch used a surface area per lipid $A \approx 66$ Å^2, whereas in these simulations $A = 62.9$ Å^2. Unfortunately, the experimental free volume fraction in lipid bilayers is not available, and previous publications using the CHARMM force field do not report the free volume distribution.

7.4. Force Fluctuation Autocorrelation Function and Friction Relaxation Times. According to eq 10, diffusion coefficients can be obtained from the time autocorrelation function of the instantaneous force fluctuation from the mean. As an example, force fluctuation autocorrelation functions for water and benzene for each of the four regions of the lipid bilayer are reported in Figure 4.

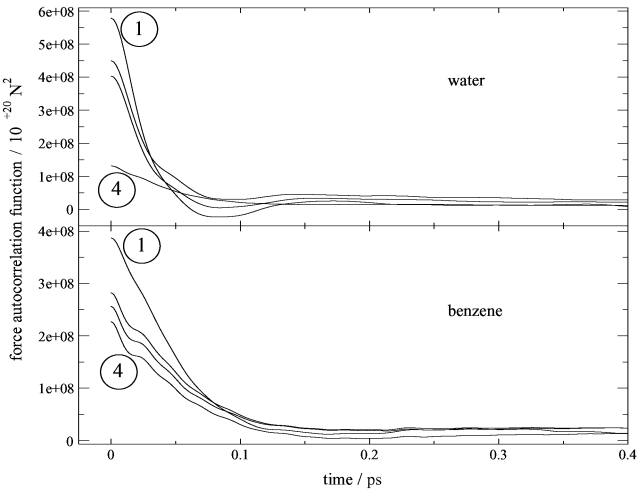

Figure 4. Force fluctuation autocorrelation functions of water and benzene. An example for each of the four regions of the lipid bilayer: moving from region 1 to region 4, $C(0)$ tend to decrease and the decay time to increase.

For these simulations, the force fluctuation time autocorrelation function was fitted with a double exponential

$$C(t) = C_1 \exp(-t/\tau_1) + C_2 \exp(-t/\tau_2) \qquad (12)$$

That a double exponential is required for a good fit to the autocorrelation function shows that solute motions inside the bilayer have two distinct time scales (τ_1 and τ_2 in eq 12). The motions with a short decay time have typical τ_{short} of 0.02−0.03 ps for water, 0.04−0.05 ps for benzene, and 0.03−0.04 ps for all of the other compounds. This corresponds to the immediate response of the solute to the local environment, i.e., the friction due to the surrounding lipids that keeps the permeants in their local cages. The value of τ_{short} tends to increase going deeper into the membrane and the value is a little higher for larger solutes. The motions with a long decay time have a typical τ_{long} of 1−12 ps. This value appears not to be systematically related to solute size. It is instead related to permeant location, as it increases moving from the lipid/water interface to region 4. This longer time-scale motion is related to the overall mechanism of diffusion through the membrane. Assuming a hopping type of diffusion, τ_{long} is related to the residence time of the penetrants in their cage of free volume between subsequent hops. Even though values for τ_{long} in regions 3 and 4 are higher, these findings are in some agreement with those of Marrink and Berendsen[37] regarding water, ammonia and oxygen permeation, where their τ_{short}s were <0.1 ps and τ_{long}s ≈ 2 ps.

7.5. Approximations. In the calculation of diffusion coefficients, it is assumed that during the decay time of the time-dependent friction coefficient the particle remains in a region of constant free energy, so that the effective friction can be fully described by considering only the static friction coefficient $\tilde{\xi}$ (see eq 7, 9, and 10). A variation in free energy of the order of RT per mole is however allowed, where R is the gas constant and T the absolute temperature, since this is the extent of thermal fluctuations. To determine whether this assumption is valid, the following calculations may be performed. Since the diffusion coefficient is related to the particle mean squared displacement, the calculated $D(z)$ can be used to obtain the mean displacement covered by the particle in a time identical to the long decay time of its friction coefficient. The difference in free energy between two positions along the bilayer normal whose distance

TABLE 1: Calculated Maximum Free Energy Difference over the Solute Displacement within the Decay Time of Its Friction Coefficient

solute	ΔG/kJ mol^{-1}
acetamide	1.33
acetic acid	1.11
benzene	0.46
ethane	0.69
methanol	0.93
methyl acetate	0.23
methylamine	0.45
water	1.41

is equal to the displacement calculated from $D(z)$, can then be compared with RT. Table 1 reports for each solute the largest free energy difference along such a distance. The reference value of RT is 2.69 kJ mol^{-1}. It is clear that for all of the compounds this approximation is valid: the change in free energy over the typical distance derived from the decay time of the friction coefficient is less than that expected for normal thermal fluctuations. In the physical picture, random motions involving the molecules of the medium give rise to impacts on the solute particle, and the response to the force acting on the particle is almost instantaneous.[50]

A second source of approximation is the fit performed on the force fluctuation autocorrelation functions shown in section 7.4. These fits are very sensitive to the parameters chosen for the exponential function (see eq 12): small changes of C_1, C_2, τ_1, and τ_2 do not yield significant changes in the correlation coefficient for the fit (so they are statistically equally acceptable) but yield different values of diffusion coefficients. Furthermore, the fitting operation is performed by minimizing the sum of the squares of the differences between the points of the fitting curve and those of the original autocorrelation function. Owing to the complex profile of the latter, the minimization algorithm can be easily trapped in a local minimum and the best fit must be found by combining automatic algorithms with manual adjustment, guided by intuition and a visual comparison of the two curves. Errors on the diffusion coefficients derived by propagation of the errors calculated from the individual autocorrelation functions[49] are comparable to those obtained by averaging the calculated diffusion coefficients over the 5 $x-y$ positions.

8. Local Resistances and Permeability Coefficients

Local resistances $\mathcal{R}(z)$ for the permeants, calculated with eq 11, are plotted in Figure 5. For clarity, error bars are not plotted. These errors are large, since, owing to the exponential form of the mathematical relationship between $\Delta G(z)$ and $\mathcal{R}(z)$, even a small error in $\Delta G(z)$ is amplified in $\mathcal{R}(z)$. Other publications[36,37] reporting $\mathcal{R}(z)$ also omit to give error bars. However, this is not a significant problem for the calculation of the overall permeability coefficient P, since this is derived from the integration of $\mathcal{R}(z)$ along the z axis from one side of the bilayer to the other. Calculated P values from these MD simulations are reported in Table 2. Where available, experimental values are also reported for comparison.

The water permeability coefficient is of the right order of magnitude with respect to the experimental data. For the other compounds with available experimental data, the discrepancy between simulation and experiment is only 1 order of magnitude, with the simulation value being higher than experiment.

Despite the fact that no experimental data are available for methanol, some extrapolations are possible. It may be surprising that the permeability for methanol, an alcohol, is lower than

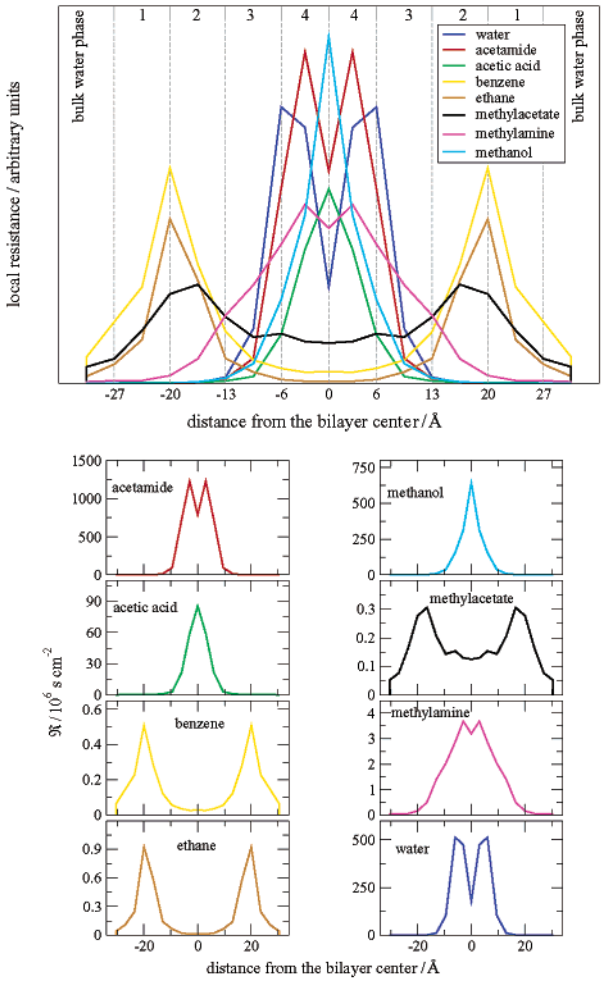

Figure 5. Local resistance profiles. For clarity, errors bars are not plotted. Top: individual profiles are arbitrarily scaled to aid comparisons. Bottom: each profile is plotted alone.

that of acetic acid. If one considers the observed apparent permeability coefficient P^{app} (see eq 1), then methanol P^{app} is indeed higher than that of acetic acid, because at common pH values the acid is mainly present as an ion, whereas the neutral form only can cross biomembranes at a significant rate. When instead considering the intrinsic permeability P_n^m of the neutral form of the solute (see eq 1 again), methanol permeability is lower than that of acetic acid. In the literature, P for ethanediol across egg PC bilayers at 25 °C is 8.8 $\times$ 10^{-5} cm s^{-1} [5,8] and P for glycerol in the same system is 5.4 $\times$ 10^{-6} cm s^{-1}.[5,8] In the same system, P for 1,2-propanediol is reported to be 2.8 $\times$ 10^{-4} cm s^{-1}, almost identical to that of 1,4-butanediol which is 2.7 $\times$ 10^{-4} cm s^{-1}.[5,8] With a crude extrapolation, P for methanol could be thought to be around 10^{-4}−10^{-3}. The value from these simulations is about 1 order of magnitude larger, as for the other compounds. For methyl acetate, the most relevant experimental data are those regarding the relative permeability of mono- and di-acetate derivatives of glycerol:[26] the partial esterification of the polyol makes P about 8 and 16 times higher, respectively. Here the esterification of methanol with acetic acid makes P of methyl acetate 2 orders of magnitude higher than that of methanol. Considering that the comparison is made with molecules whose size and number of hydroxyl groups are very different, that the esterification of glycerol in the experiments was incomplete, and that the lipid composition and the temperature of the experiments and the simulations differ, the value calculated here for methyalcetate appears of the right order of

TABLE 2: Calculated and Measured Permeability Coefficents[a]

solute	these MD simulations, 50 °C	expt egg lecithins, T °C	expt pure DPPC, T °C
actamide	$6.57\ (\pm1.92) \times 10^{-3}$	1.7×10^{-4}, 25[b] 1.7×10^{-4}, 25[d] $2.9\ (\pm0.3) \times 10^{-4}$, 25[f] $2.9\ (\pm0.3) \times 10^{-4}$, 25[g]	$\approx 4.5 \times 10^{-4}$, 48[c] 1.65×10^{-4}, 25[e]
acetic acid	$1.27\ (\pm0.55) \times 10^{-1}$	6.9×10^{-3}, 25[b] 6.6×10^{-3}, 22[i] $5.0\ (\pm0.2) \times 10^{-3}$, 25[g]	$\approx 1.1 \times 10^{-2}$, $\approx$50[h] $3.3\ (\pm0.4) \times 10^{-2}$, 50[j] $2.0\ (\pm0.4) \times 10^{-2}$, 36[k]
benzene	9.91 (±1.11)		
ethane	6.75 (±0.82)		
methanol	$1.94\ (\pm0.44) \times 10^{-2}$		
methylacetate	9.50 (±1.11)		
methylamine	1.25 (±0.16)	8.0×10^{-2}, 25[b] $\approx 9.0 \times 10^{-1}$, 50[l]	
water	$1.33\ (\pm0.28) \times 10^{-2}$	3.4×10^{-3}, 25[b] 2.2×10^{-3}, 25[d] $1.9\ (\pm0.9) \times 10^{-3}$, 25[g]	2.5×10^{-2}, 30[m] 2.2×10^{-2}, 25[e] $31.5\ (\pm1.1) \times 10^{-3}$, 37[n] $7\ (\pm3) \times 10^{-2}$, 77[o]

[a] P values are in cm s^{-1}, and T are temperatures in °C. [b] From ref 5. [c] From ref 31. [d] From ref 8. [e] From ref 7. [f] From ref 22. [g] From ref 23. [h] From ref 16. [i] From ref 4. [j] From ref 15. [k] Measured in pure DMPC. From ref 14. [l] From ref 11. The publication simply reports $P^{app} = 1.0 \times 10^{-6}$ at pH 6.7 and temperature 25 °C, and an activation energy of about 18 kcal mol^{-1}; with this information, considering methylamine $K_b = 3.38$ and assuming that only the neutral form crosses membranes at a significant rate, a value of 8.3×10^{-2} cm s^{-1} at 25 °C and the value reported in the table at 50 °C for the intrinsic permeability coefficient of the neutral form P_n^m were obtained using the equation $P^{app} = P_n^m f_n$, with f_n being the fraction of the neutral form. [m] From ref 30. [n] From ref 64. [o] Value obtained in MD simulation by Marrink and Berendsen.[36]

magnitude or may indeed be 1 order of magnitude higher, as for the other compounds.

The experimental benzene permeability was not found in the literature. These simulations yield quite a high value. However, benzoic acid has P 2 orders of magnitude higher than that of acetic acid.[4,5,23]

The discrepancy between theory and experiment, with calculated Ps being 1 order of magnitude higher than experiment, may be due to the fact that the permeation free energy surface was not sampled completely, as Klein et al. suggested in an all-atom simulation study of halothane in a DPPC bilayer.[40] However, their simulation was much shorter and no constraints were applied to the solutes.

8.1. Hydrophilic Compounds. The resistance is largely determined by the free energy profile, and the influence of diffusion coefficients seems almost negligible. As expected, the main barrier to permeation is represented by the hydrocarbon core of the membrane, where both solute partition and diffusion are less favorable than in the water phase.

8.2. Hydrophobic Compounds. For the hydrophobic compounds, the resistance profile is completely opposite. The main contribution to R is offered by the headgroup region, which is highly polar and charged. For methyl acetate, most of the resistance is due to the presence of the lipid headgroups, but regions 3 and 4 also offer a significant contribution to R. As for the hydrophilic compounds, R is primarily determined by $\Delta G(z)$.

8.3. Implications for Drug Design. Membrane permeation is clearly important for drug design and the studies reported here are relevant to this for a number of reasons. First, the methodology has been tested and validated on larger molecules than those examined in earlier work, containing chemical functionalities that are typically present in real drugs. Second, studies of such small molecules may be useful for validating the QSAR type approaches used for predicting permeability[65−67] and in particular for rationalizing situations where the QSAR approaches fail. The simulation methodology used here may of course be used to calculate the permeabilities of real drugs; these studies have been performed and will be reported elsewhere. Simulations are also likely to become increasingly important as the power of computers increases, since the practical synthesis of drug candidates and the measurement of their partition coefficients is then no longer required in a first screen.

9. Limitations and Errors

In the computational methods applied here, there are inevitably sources of error.

The force field employed may not be the most appropriate for these calculations. However, simulations of pure DPPC bilayers have been shown to yield a realistic physical picture of such systems and to reproduce the experimental data.[51,52] Therefore, this membrane computer model is expected to be a good choice for permeation studies. On the other hand, the parameters for the small organics may not be adequate. These parameters are available from the distributed version of the CHARMM force field for lipids and proteins and so are expected to be consistent with the parameters employed to model the lipid molecules. However, they are optimized for simulations in the water phase and their performance in a lipid bilayer may not be as good. It would however be necessary to optimize solute parameters at each of the membrane locations, but this is not reasonable.

A particular note must be made regarding the parameters employed to simulate methylamine. This residue, like the other compounds studied here, is present in the latest CHARMM force field for proteins,[68] which is said to be consistent with the latest CHARMM force field for lipids.[51] However, just after the simulations described here were completed and analyzed, a publication by MacKerell et al.[69] appeared with updated and refined parameters for simple amines. However, the results obtained using the old parameters are consistent with the overall trends observed.

Although bilayer anisotropy is present along the bilayer normal, and hence the force acting on a permeant varies with depth, these studies reveal that the mean forces at the same depth but different $x-y$ positions indeed differ, and complete convergence is not reached even after 2 ns. It was found that the value of $\langle \boldsymbol{F}(z) \rangle_t$ is more sensitive to the position on the bilayer plane than to the force field employed (data not shown) and therefore any bias in the starting configuration would have affected the results. In this study, it was considered appropriate

to use five independent positions per depth, and it is thought that the results are suitable for drawing fairly reliable conclusions about solute partitioning and diffusion.

When the pressure is kept constant in lipid bilayer simulations, the most obvious choice is to use an isotropic pressure ensemble, where the normal and lateral components with respect to the water/lipid interface are identical, because experiments clearly show that such a system is tension free. If the temperature is also constrained, in MD simulations, this corresponds to the *NPT* ensemble. However, it has been argued that a nonzero surface tension is appropriate to correct for the finite size of the simulation system compared with macroscopic real membranes whose experimental properties are to be reproduced.[70] It has been shown that with the CHARMM force field the $NP_N\gamma T$ and NP_NAT ensembles yield the best agreement with experiments[52,71] and are equally reliable. γ corresponds to the surface tension, and P_N corresponds to the pressure normal to the bilayer surface. For this reason, a "simpler" *NPT* ensemble seemed inappropriate for these simulations. The $NP_N\gamma T$ could therefore be chosen for these permeation studies. A fully flexible simulation cell could adjust its dimensions because of the presence of the solutes. However, the appropriate value of γ is highly sensitive to the size and the force field of the simulated system, and there is no guiding procedure for its optimization. Previous work[71] clearly demonstrates the difficulty in determining the value of γ to a high precision. For a CHARMM pure lipid bilayer, a large range for γ between 35 and 45 dyn cm^{-1} was given, but the presence of permeants is expected to alter the bilayer surface tension. This range was obtained with a 1 ns simulation, but it was noted that convergence and sufficient equilibrium sampling of area fluctuations would require a few tens of ns, and that additional inaccuracies in the potential energy parameters could significantly alter the value. Furthermore the CHARMM authors prefer using a constant surface area than constant surface tension ensemble in their work on lipid bilayers. The final choice of ensemble for these simulations was therefore NP_NAT. When a small amount of a small solute enters the membrane, the lipid structure is not altered, as shown by these and previous simulations, so that the area per lipid should also arguably remain constant. Moreover, the same packing constraints existing in pure lipid membranes are expected to still act when solutes try to permeate: these studies were not intended to understand modifications to lipid structure by solutes but rather the forces operating on solutes when permeating the membrane. However, we are aware that the bilayer surface area may increase slightly on penetration of the headgroup region by the solutes, and consequently care was taken to ensure that only one solute was present in the densest region of the bilayer for each leaflet at any one time.

The use of a nonflexible simulation cell for simulating solute diffusion within lipid bilayers is not new. Stouch et al. performed such simulations using a constant volume/constant temperature ensemble and also employed the same value of surface area per lipid for both pure DMPC bilayers[72,73] and solute/membrane systems.[44,45,47]

10. Conclusions

In this article, permeability coefficients for eight small organic molecules representing the most common chemical functional groups have been calculated by means of MD simulations and compared with available experimental data. Calculated values are generally 1 order of magnitude higher, but the rank ordering of the molecules is correct.

The distinguishing feature of the solubility-diffusion model is that it incorporates information about both the equilibrium and the dynamic behavior of the solute in the bilayer. Equilibrium properties are described by the free energy, which depends on the magnitude and the direction of the mean force acting on the permeant molecule and yields the solute ability to partition into the membrane from water. Dynamic properties are described by the diffusion coefficient, which depends on the amplitude of the fluctuations of the instantaneous force from the mean and on its relaxation time, and yields the ability of the solute to move inside the membrane from one side to the other. The advantage of MD simulations is that the different contributions from the different regions of the lipid bilayer, that is free energy, diffusion, and local resistance as a function of z, can be studied at a molecular level, whereas experiments can only approximate the membrane as a uniform barrier slab.

In general, the solute free energies increase on moving from the water phase into the membrane, probably due to the increase in local density. For the hydrophilic solutes, the free energy continues to increase on entering the hydrocarbon core of the membrane, whereas for the hydrophobic solutes, the converse is true. Interestingly, methyl acetate behaves as a hydrophobic solute, perhaps due to the absence of hydrogen bond donors on the molecule resulting in no hydrogen bonding with the lipids. There is in general a good correlation between the free energy in the center of the membrane with the experimental free energy of partitioning for the solute between water and hexadecane. The notable exception to this rule is for benzene, which, because of its size, is sensitive to the lateral packing in the lipid bilayers, supporting the view that biomembranes do not always behave like bulk solvents.

Diffusion coefficients decrease significantly for all molecules on entering the membrane but show a slight increase at the very center of the bilayer, presumably because of the lower density at this location. With the exception of water, the diffusion coefficients of the molecules are broadly similar.

In this article, it has been shown that the solubility-diffusion model as applied in the context of molecular dynamics computer simulations is able to reproduce the relative permeabilities of eight small molecules representing common chemical functionalities. An article reporting the application of this methodology to drug molecule permeation will be submitted shortly.

Acknowledgment. We should like to thank the EPSRC for supporting this work. D.B. thanks Aventis for their generous support. Also, thanks to I.C. Walton, I.D. Hardy, and O.G. Parchment for their help in running the simulations on the Southampton University PC cluster, IRIDIS (http://www.sucs.soton.ac.uk/research/iridis/).

References and Notes

(1) Balaz, S. *Perspect. Drug Discovery Des.* **2000**, *19*, 157−177.
(2) Singer, S.; Nicolson, G. L. *Science* **1972**, *172*, 720−730.
(3) Bean, R. C.; Shepherd, W. C.; Chan, H. *J. Gen. Physiol.* **1968**, *52*, 495−508.
(4) Walter, A.; Gutknecht, J. *J. Membr. Biol.* **1984**, *77*, 255−264.
(5) Walter, A.; Gutknecht, J. *J. Membr. Biol.* **1986**, *90*, 207−217.
(6) Wolosin, J. M.; Ginsburg, H. *Biochim. Biophys. Acta* **1975**, *389*, 20−33.
(7) Finkelstein, A. *J. Gen. Physiol.* **1976**, *68*, 127−135.
(8) Orbach, E.; Finkelstein, A. *J. Gen. Physiol.* **1980**, *75*, 427−436.
(9) Brunner, J.; Graham, D. E.; Hauser, H.; Semenza, G. *J. Membr. Biol.* **1980**, *57*, 133−141.
(10) Gutknecht, J.; Walter, A. *Biochim. Biophys. Acta* **1981**, *649*, 149−154.
(11) Bar-On, Z.; Degani, H. *Biochim. Biophys. Acta* **1985**, *813*, 207−217.
(12) Bochain, A.; Estey, L.; Haronian, G.; Reale, M.; Rojas, C.; Cramer, J. *J. Membr. Biol.* **1981**, *60*, 73−76.
(13) Lande, M. B.; Donovan, J. M.; Zeidel, M. L. *J. Gen. Physiol.* **1995**, *106*, 67−84.

(14) Xiang, T. X.; Anderson, B. D. *J. Membr. Biol.* **1995**, *148*, 157−167.
(15) Xiang, T. X.; Anderson, B. D. *Biophys. J.* **1997**, *72*, 223−237.
(16) Xiang, T. X.; Anderson, B. D. *Biophys. J.* **1998**, *75*, 2658−2671.
(17) Xiang, T. X.; Anderson, B. D. *Biochim. Biophys. Acta* **1998**, *1370*, 64−76.
(18) Bresseleers, G. J. M.; Goderis, H. L.; Tobback, P. P. *Biochim. Biophys. Acta* **1984**, *772*, 374−382.
(19) Dix, J. A.; Kivelson, D.; Diamond, J. M. *J. Membr. Biol.* **1978**, *40*, 315−342.
(20) Xiang, T. X.; Anderson, B. D. *J. Membr. Biol.* **2000**, *173*, 187−201.
(21) Xiang, T. X.; Anderson, B. D. *J. Membr. Biol.* **2000**, *177*, 137−148.
(22) Xiang, T. X.; Chen, X.; Anderson, B. D. *Biophys. J.* **1992**, *63*, 78−88.
(23) Xiang, T. X.; Anderson, B. D. *J. Membr. Biol.* **1994**, *140*, 111−122.
(24) Bindslev, N.; Wright, E. M. *J. Membr. Biol.* **1976**, *29*, 265−288.
(25) Cohen, B. E. *J. Membr. Biol.* **1975**, *20*, 205−234.
(26) Cohen, B. E. *J. Membr. Biol.* **1975**, *20*, 235−268.
(27) Diamond, J. M.; Katz, Y. *J. Membr. Biol.* **1974**, *17*, 121−154.
(28) Todd, A. P.; Mehlhorn, R. J.; Macey, R. I. *J. Membr. Biol.* **1989**, *109*, 41−52.
(29) Xiang, T. X.; Anderson, B. D. *J. Membr. Biol.* **1998**, *165*, 77−90.
(30) Paula, S.; Volkov, A. G.; Van Hoek, A. N.; Haines, T. H.; Deamer, D. W. *Biophys. J.* **1996**, *70*, 339−348.
(31) Hill, W. G.; Rivers, R. L.; Zeidel, M. L. *J. Gen. Physiol.* **1999**, *114*, 405−414.
(32) Berendsen, H. J. C.; Marrink, S. J. *Pure Appl. Chem.* **1993**, *65*, 2513−2520.
(33) Overton, E. *Vierteljahrschr. Naturforsch. Ges. Zurich* **1895**, *40*, 159−201.
(34) De Young, L. R.; Dill, K. A. *Biochemistry* **1988**, *27*, 5281−5289.
(35) De Young, L. R.; Dill, K. A. *J. Phys. Chem.* **1990**, *94*, 801−809.
(36) Marrink, S. J.; Berendsen, H. J. C. *J. Phys. Chem.* **1994**, *98*, 4155−4168.
(37) Marrink, S. J.; Berendsen, H. J. C. *J. Phys. Chem.* **1996**, *100*, 16729−16738.
(38) McKinnon, S. J.; Whittenburg, S. L.; Brooks, B. *J. Phys. Chem.* **1992**, *96*, 10497−10506.
(39) Pohorille, A.; Wilson, M. A. *J. Chem. Phys.* **1996**, *104*, 3760−3773.
(40) Tu, K.; Tarek, M.; Klein, M. L.; Scharf, D. *Biophys. J.* **1998**, *75*, 2123−2134.
(41) Pohorille, A.; New, M. H.; Schweighofer, K.; Wilson, M. A. *Curr. Top. Membr.* **1999**, *48*, 49−76.
(42) Xiang, T. X. *J. Phys. Chem. B* **1999**, *103*, 385−394.
(43) Koubi, L.; Tarek, M.; Klein, M. L.; Scharf, D. *Biophys. J.* **2000**, *78*, 800−811.
(44) Bassolino-Klimas, D.; Alper, H. E.; Stouch, T. R. *J. Am. Chem. Soc.* **1995**, *117*, 4118−4129.
(45) Bassolino-Klimas, D.; Alper, H. E.; Stouch, T. R. *Biochemistry* **1993**, *32*, 12624−12637.
(46) Stouch, T. R.; Alper, H. E.; Bassolino, D. *J. Comput.-Aided Mol. Des.* **1995**, *589*, 127−138.
(47) Alper, H. E.; Stouch, T. R. *J. Phys. Chem.* **1995**, *99*, 5724−5731.
(48) Ryckaert, J. P.; Ciccotti, G.; Berendsen, H. J. C. *J. Comput. Phys.* **1977**, *23*, 327−341.
(49) Roux, B.; Karplus, M. *J. Phys. Chem.* **1991**, *95*, 4856−4868.
(50) Kubo, R. *Rep. Prog. Phys.* **1966**, *29*, 255−284.
(51) MacKerell, A. D.; Feller, S. E. *J. Phys. Chem. B* **2000**, *104*, 7510−7515.
(52) Feller, S. E.; Venable, R. M.; Pastor, R. W. *Langmuir* **1997**, *13*, 6555−6561.
(53) Hockney, R. W. *Methods Comput. Phys.* **1970**, *9*, 136−211.
(54) Feller, S. E.; Zhang, Y.; Pastor, R. W.; Brooks, B. R. *J. Chem. Phys.* **1995**, *103*, 4613−4621.
(55) Hoover, W. G. *Phys. Rev. A* **1985**, *31*, 1695−1697.
(56) Brooks, B. R.; Bruccoleri, R. E.; Olafson, B. D.; States, D. J.; Swaminathan, S.; Karplus, M. *J. Comput. Chem.* **1983**, *4*, 187−217.
(57) Zhu, T.; Li, J.; Hawkins, G. D.; Cramer, C. J.; Truhlar, D. G. *J. Chem. Phys.* **1998**, *109*, 9117−9133.
(58) Chipot, C.; Wilson, M. A.; Pohorille, A. *J. Phys. Chem. B* **1997**, *101*, 782−791.
(59) Pohorille, A.; Wilson, M. A.; New, M. H.; Chipot, C. *Toxicol. Lett.* **1998**, *100−101*, 421−430.
(60) Pratt, L. R.; Pohorille, A. *Chem. Rev.* **2002**, *102*, 2671−2692.
(61) McIntosh, T. J.; Simon, S. A.; MacDonald, R. C. *Biochim. Biophys. Acta* **1980**, *597*, 445−463.
(62) White, S. H.; King, G. I.; Cain, J. E. *Nature* **1981**, *290*, 161−163.
(63) Katz, Y.; Diamond, J. M. *J. Membr. Biol.* **1974**, *17*, 101−120.
(64) Graziani, Y.; Livne, A. *J. Membr. Biol.* **1972**, *7*, 275−284.
(65) Palm, K.; Luthman, K.; Ungell, A.; Strandlund, G.; Beigi, F.; Lundhal, P.; Artursson, P. *J. Med. Chem.* **1998**, *41*, 5382−5392.
(66) Clark, D. E. *J. Pharm. Sci.* **1999**, *88*, 807−814.
(67) Clark, D. E. *J. Pharm. Sci.* **1999**, *88*, 815−821.
(68) MacKerell, A. D.; Yin, D.; Roux, B.; Karplus, M. *J. Phys. Chem. B* **1998**, *102*, 3586−3616.
(69) Chen, I. J.; Yin, D.; MacKerell, A. D. *J. Comput. Chem.* **2002**, *23*, 199−213.
(70) Feller, S. E.; Pastor, R. W. *Biophys. J.* **1996**, *71*, 1350−1355.
(71) Feller, S. E.; Pastor, R. W. *J. Chem. Phys.* **1999**, *111*, 1281−1287.
(72) Stouch, T. R. *Mol. Sim.* **1993**, *10*, 335−362.
(73) Stouch, T. R.; Alper, H. E.; Bassolino-Klimas, D. *Supercomput. Appl. High Perform. Comput.* **1994**, *8*, 6−23.